EXTRACTION OF PEPPERMINT OIL BY SUPERCRITICAL CARBON DIOXIDE

MOTONOBU GOTO*, MASAKI SATO
AND TSUTOMU HIROSE
Department of Applied Chemistry, Kumamoto University, Kumamoto 860

Key Words: Extraction, Supercritical Fluid, Peppermint Oil, Carbon Dioxide, Extraction Rate, Mathematical Model, Adsorption, Mass Transfer

The extraction of essential oil from peppermint leaves with supercritical carbon dioxide was studied in a semibatch-flow extraction apparatus. The extraction rates of the major components, *l*-menthol and menthone, were measured at various conditions: 313-353 K, 8.83-19.6 MPa. The exit concentration of *l*-menthol extracted from peppermint leaves was much smaller than the solubility of *l*-menthol. The extraction curves at various flow rates coincide in the plot of yield versus quantity of CO_2 consumed. A mathematical model based on the local adsorption equilibrium of essential oil on lipid in leaves and mass transfer well described the extraction results. The adsorption equilibrium constant determined by fitting the theoretical extraction curve to the experimental data increased with temperature and decreased with pressure.

Introduction

Steam distillation, expression and solvent extraction have been used for the isolation of essential oils from plant materials. Most essential oils such as mint oils have been predominantly recovered by steam distillation. Although that method has been widely applied, it has some disadvantages: the heat instability of essential oils, and the fact that only volatile components can be isolated, which sometimes leads to instability of product oil. Expression is applied in limited cases such as the production of citrus oil. Solvent extraction is useful for the full extraction of chemicals in plants, but denaturation by a solvent and the difficulty of removing the solvent from product oil are inevitable problems.

Supercritical fluid extraction has become a focus of interest in the field of extraction from natural materials. Supercritical fluid has advantages such as excellent mass transfer properties and ease of control of solubility by temperature, pressure or entrainer. Carbon dioxide is mainly used because of its near ambient critical temperature, absence of residual problems and the inexpensive, odorless, colorless, nontoxic, nonflammable, and noncorrosive nature of the solvent.

The dissolving power of a supercritical fluid depends significantly on the temperature and pressure[2]. At lower pressure near the critical point, only volatile components, such as essential oils, are extracted, while total extracts including fats, waxes, resins and dyes are extracted at higher pressure where the fluid has a liquid-like density.

The extraction of natural solid materials involves dissolution of solid component, diffusion in cellular material and external mass transfer around the solid particle. A diffusion model has been used to explain the extraction rate of caffeine from coffee beans[3]. Peker *et al.*[8] used a mathematical model based on mass transfer and partitioning of caffeine between the water phase and the supercritical fluid phase to explain the extraction of caffeine from water-soaked beans. The extraction behavior of adsorbed solute from an adsorbent such as activated carbon has been explained by intraparticle and external mass transfer with linear or nonlinear adsorption-desorption kinetics[10, 11].

The objective of this work is to study the extraction of essential oil from plant materials and to analyze the dynamic behavior of the extraction by a mathematical model in a manner similar to that employed by Peker *et al.*[8] and Srinivasan *et al.*[10]

1. Experiments

1.1 Experimental apparatus

The experimental apparatus is schematically shown in **Fig. 1**. Carbon dioxide from a cylinder with siphon attachment is passed through a cooling bath and compressed to the operating pressure by a HPLC pump (Jasco, PU-980). The flow rate of the fluid is regulated at the HPLC pump. The compressed fluid is passed through a constant-temperature water bath and then flows to the extractor column in the water bath. The fluid exiting from the extractor is expanded to ambient pressure through a back-pressure regulator (Jasco, PC880-81) and bubbled in a cold ethanol trap to collect extracted materials. For runs with entrainer, 2 - 6 wt% of ethanol was mixed with carbon dioxide by pumping ethanol into the carbon dioxide line with the HPLC pump. To prevent deposition of extracts beneath the back-pressure regulator, another HPLC pump supplies ethanol into the line before entry into the back-pressure regulator.

* Received December 21, 1992. Correspondence concerning this article should be addressed to M. Goto.

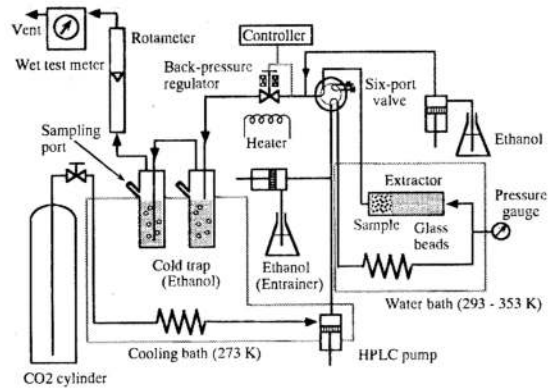

Fig. 1 Experimental apparatus

The pressure in the extractor is controlled by the back-pressure regulator.

The composition in the ethanol trap is analyzed with a gas chromatograph (Yanaco, G2800) equipped with FID detector and *G*-column (G-100, 40m × 1.2 mm i.d.).

The extractor column is 50 mm long and 23 mm i.d. Dried peppermint leaves are packed in the column. The void space is filled with glass beads to reduce the dead space and make the flow uniform in the extractor column. To prevent channeling of the flow in the packed bed, the peppermint leaves are crushed into pieces around 3 mm square and stored in a desiccator.

1.2 Experimental procedure

About 2 g of dried peppermint leaves were placed in the extractor column for the extraction run. At the beginning the six-port valve was set so that the carbon dioxide passes the back-pressure regulator without passing through the extractor column. After the pressure and the flow rate reached the desired values, the six-port valve was switched so that carbon dioxide passed through the extractor column to start the extraction. Soon after the desired pressure was regained, the flow of ethanol into the line was started at the back-pressure regulator to prevent deposition of extracts.

A small amount of solution from the ethanol trap was withdrawn by microsyringe in a certain interval to measure the concentration of components. To confirm that whole components extracted were collected without dissipation by gas flow, three ethanol traps were placed in series. Depending on the operating condition, some components were detected in the second trap. However, one trap was enough to collect all extracts in most extraction runs.

The extraction runs were carried out in a temperature range of 293 - 353 K, a pressure range of 8.82-19.6 MPa, and a flow rate of $3.3 - 13 \times 10^{-8}$ m^3/s at a pump condition (ca. 273 K) corresponding to $3.2 - 12.8 \times 10^{-5}$ kg/s.

The solubility of *l*-menthol in supercritical carbon dioxide was measured with the same apparatus used for peppermint extraction in the following manner. Crushed crystals of pure *l*-menthol were placed in the extractor column. Extraction of *l*-menthol was carried out at a flow rate of 3.2×10^{-5} kg/s and various pressures and temperatures. This measurement was based on the assumption that the flow rate was slow enough to reach equilibrium solubility within the extractor so that the concentration in the cold ethanol trap increases linearly with time. This assumption was confirmed to be valid by changing the flow rate ($3 - 6 \times 10^{-5}$ kg/s).

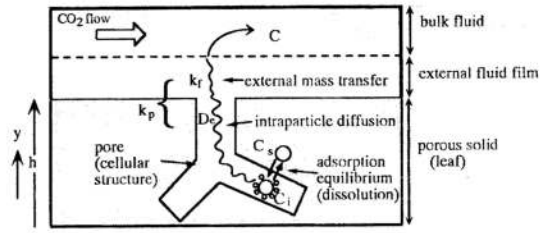

Fig. 2 Schematic diagram of extraction mechanism

2. Mathematical Model

Dried peppermint leaves are comprised of structural materials such as cellulose and the other components such as essential oil, lipid and protein. The extractable components are mainly essential oil and some lipid. As discussed later, the lipid may influence the extraction of essential oils. From the viewpoint of engineering application, we prefer a simpler model to an exact but complicated model.

We make the following assumptions. 1) Peppermint leaves are a porous solid which involves essential oils and lipid. 2) Essential oils are extracted from leaves as if desorbed from solid biotissue where lipid is associated with essential oils. 3) Essential oils dissolved in supercritical fluid diffuse to the external surface and through the external film to be carried away by bulk flow. **Figure 2** shows the schematic extraction process.

Consider a differential bed containing particles of slab geometry, with an initial concentration of solute in the leaf, $C_{s,0}$. Pure solvent enters the bed, the pore and void volumes are initially free of solute, and the process is isothermal. The governing equations are as follows.

The mass balance for the solute in the bulk solvent in the differential, continuous-flow extractor column is:

$$\alpha \frac{\partial C}{\partial t} + \frac{C}{\tau} = -(1-\alpha) k_f a_p [C - (C_i)_{y=h}] \tag{1}$$

where τ refers to a residence time, given as the total bed volume divided by the volumetric flow rate of supercritical fluid at the conditions of the extractor column, and thickness of the slab is $2h$. Specific surface area a_p is given by $a_p = 1/h$.

The mass balance for the solute in the pores is:

$$\beta \frac{\partial C_i}{\partial t} = D_e \frac{\partial^2 C_i}{\partial y^2} - (1-\beta) \frac{\partial C_s}{\partial t} \tag{2}$$

The local extraction rate, which is equivalent to the desorption rate, is assumed to be reversible and linear.

$$\frac{\partial C_s}{\partial t} = k_a\left(C_i - \frac{C_s}{K}\right) \tag{3}$$

in terms of the adsorption rate constant k_a and the adsorption equilibrium constant K.

The initial and boundary conditions are:

$$D_e\left(\frac{\partial C_i}{\partial y}\right)_{y=h} = k_f\left[C - (C_i)_{y=h}\right] \tag{4}$$

$$C(y, t=0) = C_i(y, t=0) = 0 \tag{5}$$

$$C_s(y, t=0) = C_{s,0} \tag{6}$$

It is assumed here that the combined internal and external mass transfer processes are described by a linear driving-force approximation[5], which is derived by assuming a parabolic concentration profile within the particle. The overall mass-transfer coefficient for a slab geometry is given by

$$k_p = \frac{k_f}{1 + Bi/3} \tag{7}$$

where the Biot number, $Bi = k_f h / D_e$. Average intraparticle concentrations are evaluated using the parabolic profile.

$$\bar{C}_i = \frac{1}{h}\int_0^h C_i(y)\,dy \tag{8}$$

In terms of average concentration $\bar{C}_i$, the mass conservation equations become

$$\alpha\frac{dC}{dt} + \frac{C}{\tau} = -(1-\alpha)k_p a_p\left(C - \bar{C}_i\right) \tag{9}$$

$$\beta\frac{d\bar{C}_i}{dt} = k_p a_p\left(C - \bar{C}_i\right) - (1-\beta)\frac{d\bar{C}_s}{dt} \tag{10}$$

$$\frac{d\bar{C}_s}{dt} = k_a\left(\bar{C}_i - \frac{\bar{C}_s}{K}\right) \tag{11}$$

It is supposed here that equilibrium in the pores is established instantaneously for a relatively fast adsorption-desorption rate,

$$\bar{C}_s = K\,\bar{C}_i \tag{12}$$

Combining Eqs. (10) and (12) to eliminate $\bar{C}_i$, yields

$$\left[\frac{\beta}{K} + (1-\beta)\right]\frac{d\bar{C}_s}{dt} = k_p a_p\left(C - \frac{\bar{C}_s}{K}\right) \tag{13}$$

In the equilibrium case, the total initial solute concentration existing both in solid phase and within the pore is given by

$$C_0 = \left[\frac{\beta}{K} + (1-\beta)\right]C_{s,0} \tag{14}$$

In terms of dimensionless variables, the above equations can be written as

$$\frac{dx}{d\theta} + \frac{x}{\alpha} = -\frac{\phi(1-\alpha)}{\alpha}\left(x - \frac{x_s}{K}\right) \tag{15}$$

$$\frac{dx_s}{d\theta} = \frac{\phi(x - x_s/K)}{[\beta/K + (1-\beta)]} \tag{16}$$

Initial conditions are

$$x(\theta = 0) = 0 \tag{17}$$

$$x_s(\theta = 0) = \frac{K}{[\beta + (1-\beta)K]} \tag{18}$$

where $x = C / C_0$, $x_s = \bar{C}_s / C_0$, $\theta = t / \tau$, and $\phi = k_p a_p \tau$.

The solution to Eqs. (15)-(18) is:

$$x(\theta) = A\left[\exp(a_1\,\theta) - \exp(a_2\,\theta)\right] \tag{19}$$

where

$$a_1 = \frac{1}{2}\left(-b + \sqrt{b^2 - 4c}\right),\ a_2 = \frac{1}{2}\left(-b - \sqrt{b^2 - 4c}\right) \tag{20}$$

$$A = \frac{(1-\alpha)\phi}{[\beta + (1-\beta)K]\,\alpha(a_1 - a_2)} \tag{21}$$

with b and c defined as

$$b = \frac{\phi}{\beta + (1-\beta)K} + \frac{1}{\alpha} + \frac{\phi(1-\alpha)}{\alpha},$$
$$c = \frac{\phi}{[\beta + (1-\beta)K]\,\alpha} \tag{22}$$

These equations are equivalent to the special case (m = 1) of the model developed by Peker *et al.*[8] for caffeine extraction. The cumulative fraction of solute extracted up to dimensionless time θ is given by

$$F(\theta) = \frac{1}{1-\alpha}\int_0^\theta x\,d\theta$$
$$= \frac{A}{1-\alpha}\left[\frac{\exp(a_1\,\theta) - 1}{a_1} - \frac{\exp(a_2\,\theta) - 1}{a_2}\right] \tag{23}$$

When mass transfer resistance is negligible, that is, when $\phi = \infty$, Eq. (23) reduces to

$$F(\theta) = 1 - \exp\left\{-\frac{\theta}{[\beta + (1-\beta)K](1-\alpha) + \alpha}\right\} \tag{24}$$

3. Results and Discussion

3.1 Solubility of *l*-menthol

The extraction measurement with pure *l*-menthol crystal solid gave the amount of *l*-menthol extracted as a function of extraction time. Since the extracted amount increased linearly with time and was not affected by changing flow rate, the concentration leaving the extractor was constant during a run, which means that equilibrium is established in the extractor. The concentration leaving the extractor corresponds to the solubility at that condition. Thus, solubilities of *l*-menthol were calculated from the slops of the extraction curve.

Figure 3 shows the measured solubilities at various pressures and temperatures. The solubility

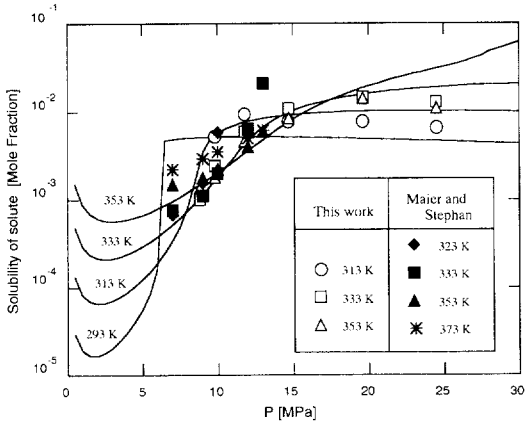

Fig. 3 Solubility of *l*-menthol in carbon dioxide (solid curves are estimated by Peng-Robinson EOS[9])

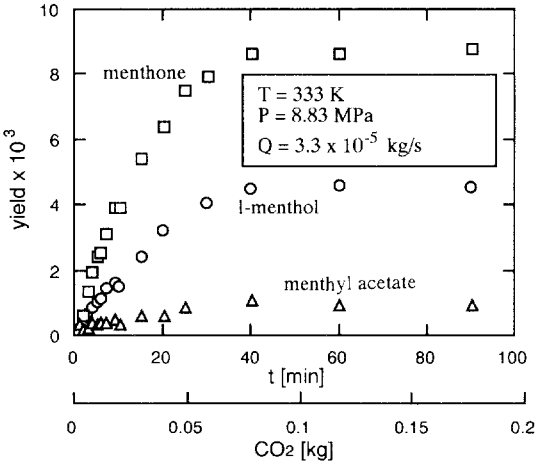

Fig. 4 Extraction curve of peppermint leaves

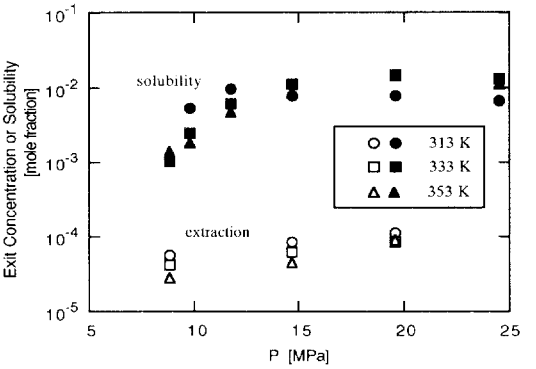

Fig. 5 Comparison between initial exit concentration of *l*-menthol for the extraction of peppermint and the solubility

decreases as temperature increases at pressures of 8 to 12 MPa, but increases as temperature increases at pressures above 15 MPa. The solubility increases with pressure up to around 10-20 MPa depending on the temperature and decreases as pressure further increases. Therefore, the highest solubility was observed around 10-20 MPa depending on the temperature. The solubilities reported by Maier and Stephan[6] are compared in Fig. 3. They almost agree with values of this work except for higher pressure at 333 K.

3.2 Dynamic behavior of extraction of peppermint

Peppermint oil consists of a variety of components such as *l*-menthol, menthone, menthyl acetate, menthofuran, pinene, 1,8-cineole, etc.[1] The composition of the oil strongly depends on the harvest place and time, the drying method of the raw leaves, and the extraction process and its condition. Barton[1] showed that the composition of oil is almost the same between steam-distilled and supercritical CO_2 extracted. The major constituents are *l*-menthol and menthone. The content of other components is less than 10%.

Typical extraction curves for *l*-menthol, menthone and menthyl acetate are shown in **Fig. 4**. The yield [kg/kg] is defined as amount extracted per unit mass of dried peppermint leaves. The yield increased almost linearly at the beginning of the run. It is interesting that these three components behaved similarly regardless of the initial content. When the yields are reduced by the final yield, the curves of reduced yield versus time almost coincide with each other. The extraction of these components was completed in the same time, around 40 min.

Ozer *et al.*[7] analyzed the extracted components of spearmint leaves in detail. They found that monoterpenes are preferably extracted at the beginning and that other components such as mono-cyclic terpene ketone, bicyclic sesquiterpene and cyclic terpene ketone are preferentially extracted later. Combining the results of our experimental work, components having similar structure were extracted similarly while components having different structures were extracted at different rates.

The concentrations in the exit fluid are calculated from the slope of the linear part of the extraction curves. The exit concentrations of *l*-menthol extracted from peppermint leaves are compared with the solubility previously shown in **Fig. 5**. The exit concentration, which corresponds to the extraction rate, is higher at lower temperature and higher pressure. However, the exit concentrations are considerably smaller than the solubility. This discrepancy may be due to one of the following reasons.

The solubility data correspond to the phase equilibria for the pure *l*-menthol/carbon dioxide system, while the extraction data were obtained from a multicomponent mixture/carbon dioxide system. The fluid-phase concentration for single component/fluid system might be different from that of the multi-components/fluid system because of a mutual entrainment effect.

When equilibrium is not attained in the extractor, the concentration leaving the extractor is smaller than equilibrium value. The extraction rate might be affected by the dissolving process or mass transfer process within the particle or in the external film. Another possible explanation is that high-boiling point components such as lipids which exist in biotissue affect the phase equilibria. The essential oil components maybe exist with lipid at the same place. In other words, the essential oils are adsorbed in lipid. The phase equilibria for this situa-

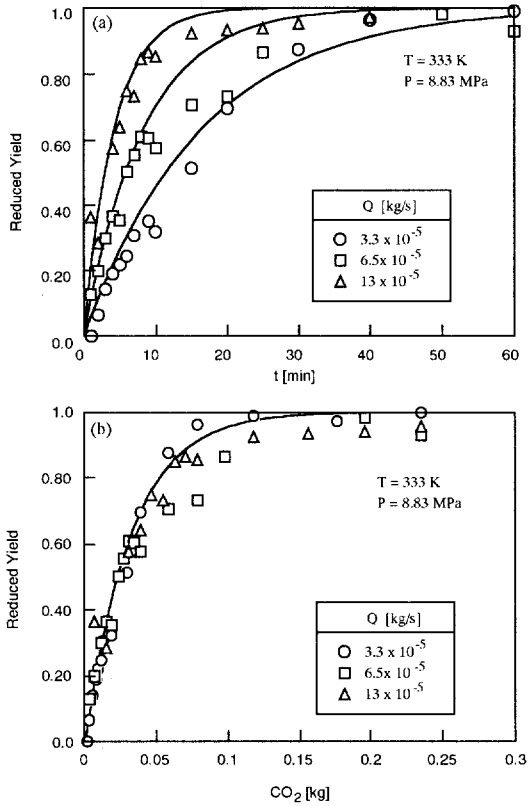

Fig. 6 Effect of flow rate on extraction of *l*-menthol (solid lines indicate predicted curves)

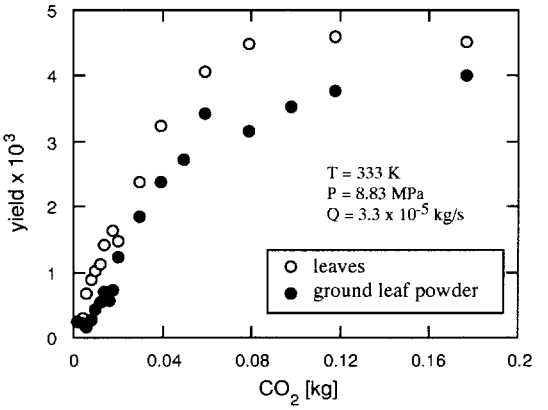

Fig. 7 Effect of particle size on extraction of *l*-menthol

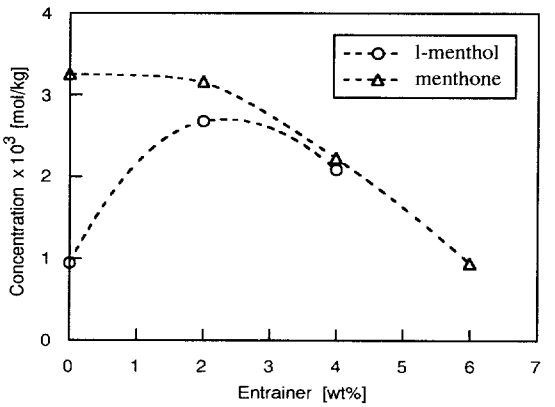

Fig. 8 Effect of entrainer on extraction rate (expressed as extracted concentration) at 8.83 MPa, 333 K and 3.2×10^{-5} kg/s

tion correspond to the adsorption equilibria of essential oil on lipid. In that case, essential oil components must be desorbed from lipid in which essential oil components are adsorbed.

One of the evident adsorption phenomena was observed in the following situation. When ethanol was not flowing at the back-pressure regulator, the apparent extraction rate of the essential oils was extremely slow, because extracted lipid was deposited in the valve and tubes after pressure reduction to atmospheric level, causing adsorption of extracted essential oil in the lipid. Deposition of solid material such as wax was observed in the tube downstream of the back-pressure regulator. Thus, the observed extraction rate was for the desorption process from lipid at atmospheric pressure. The mathematical model developed above is based on this phenomenon.

We consider here the effect of mass transfer on the extraction process. The extraction curve from solid material is usually reported to be linear at the beginning, then changing to a logarithmic curve[3]. This behavior has been considered to be due to the effect of mass transfer.

Figure 6 shows the effect of flow rate on the extraction of *l*-menthol at 333 K and 8.83 MPa. The reduced yields are plotted as a function of extraction time in Fig. 6 (a) and are plotted in Fig. 6 (b) as a function of the amount of carbon dioxide consumed. The reduced yield is defined as the ratio of yield to final yield. Since the final yield does not accurately reflect the same value, reduced yield was used for the purpose of comparison. As can be seen in Fig. 6 (a) the extraction rate is higher for larger flow rate. On the other hand, the extraction rate in the plot of Fig. 6 (b) is not affected by flow rate at the beginning of the extraction run. This indicates that the exit concentration of extracts is independent of flow rate, at least at the beginning, and therefore equilibrium is considered to hold. If intraparticle diffusion resistance is important, the slopes of the extraction curve in the plot of yield versus CO_2 become smaller for higher flow rate. If the external mass transfer affects the extraction process as in the case of desorption from activated carbon[10], the curve for lower flow rate becomes gentler in Fig. 6 (b). Therefore, the reason why the extraction curves deviate from a straight line does not seem to be the effect of mass transfer limitation.

To confirm the above findings, extraction experiments were carried out with peppermint leaf powder ground in a porcelain mortar. A comparison of the extraction curve between ground and non-ground samples is shown in **Fig. 7**. Since a considerable menthol-like smell was observed during the grinding process, some extractable components dissipate from the leaves, resulting in the disagreement of the final yield. The extraction curves are very similar to each other. Therefore, the phenomena of decreasing extraction rate, that

Table 1. Extraction conditions and estimated parameters

T [K]	P [MPa]	ρ [kg/m^3]	$\mu \times 10^5$ [kg/m·s]	$Q \times 10^5$ [kg/s]	Re [-]	$k_f \times 10^4$ [m/s]	$D_e \times 10^9$ [m^2/s]	Bi [-]	$k_p \times 10^4$ [m/s]
313	8.83	411	2.77	3.27	0.459	4.80	7.01	5.13	1.77
313	14.7	787	6.29	3.38	0.208	1.71	2.57	5.00	0.642
313	19.6	849	7.37	3.44	0.181	1.16	1.70	5.13	0.428
333	8.83	227	2.17	3.27	0.584	7.97	11.2	5.31	2.88
333	14.7	577	3.92	3.38	0.334	3.29	4.92	5.02	1.23
333	19.6	720	5.43	3.44	0.246	2.33	3.52	4.96	0.878
353	8.83	183	2.15	3.27	0.591	10.3	14.6	5.29	3.72
353	14.7	406	2.94	3.38	0.445	4.63	6.72	5.16	1.70
353	19.6	574	4.00	3.44	0.334	3.26	4.85	5.04	1.22
333	8.83	227	2.17	6.54	1.17	9.41	11.2	6.27	3.04
333	8.83	227	2.17	13.1	2.34	11.6	11.2	7.73	3.24

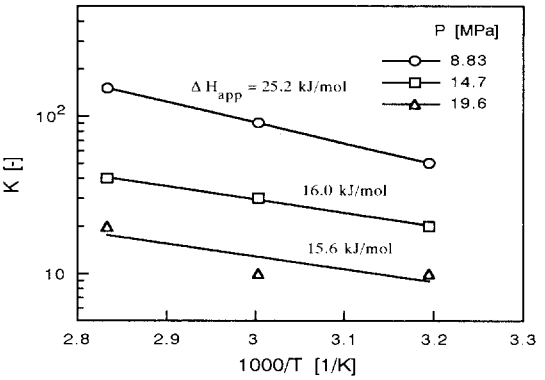

Fig. 9 Adsorption equilibrium constants

is, deviation from the straight line, cannot be explained by the intraparticle mass transfer resistance.

Both the slow-dissolving rate model and the adsorption model may be able to explain these phenomena. In conjunction with the effect of adsorption in lipid mentioned above, we analyze the data by the adsorption/desorption model with mass transfer.

3.3 Effect of entrainer

The effect of entrainer on the initial extraction rate is shown in **Fig.8**. When 2 wt% ethanol in carbon dioxide was used as an entrainer, the extraction rate of *l*-menthol was increased threefold, while the extraction rate of menthone was not affected. The extraction rates of both *l*-menthol and menthone were decreased with further increase in the concentration of entrainer. The final extraction yield was not affected by the entrainer. Since extracts with 6 wt% entrainer had darker color and wax, further increase of ethanol accelerates the extraction of coloring pigments such as chlorophyll and lipid, resulting in a reduction of the extraction rate of essential oils.

3.4 Estimation of properties for theoretical analysis

Properties of supercritical carbon dioxide under the operating conditions are listed in **Table 1**. The density was estimated by the method used by Goto *et al.*[4] The binary diffusion coefficient of *l*-menthol was estimated by Reid *et al.*[9] with Takahashi's correlation. The external mass transfer coefficient k_f was estimated by the Wakao and Kaguei correlation[12]. The effective intraparticle diffusion coefficient was estimated as $D_e = D_{AB}\,\beta^2$.

The physical properties of peppermint leaf were measured. The solid density, apparent density and specific surface area of the leaf were ρ_s = 1460 kg/m^3, ρ_p = 676 kg/m^3 and a_p = 1.3 × 10^4 1/m, respectively. The porosity of the leaf was calculated with these values to be $\beta = 1 - \rho_p / \rho_s = 0.538$. The bed void fraction was α = 0.745.

3.5 Analyses of experimental extraction curve by the model

The experimental extraction rate was analyzed by the local equilibrium model where the overall mass transfer coefficient k_p and adsorption equilibrium constant K were involved as parameters. Since the mass transfer coefficient was estimated by the correlation, the parameter which must be determined is the adsorption equilibrium constant, K. The theoretical extraction curve and experimental curve were fitted visually on PC graphics with the adsorption equilibrium constant, K, as a fitting parameter. When the values of the overall mass transfer coefficient, k_p, estimated above were used, the mass transfer resistance did not affect the extraction curve. Mass transfer in both particles and external film was so fast that adsorption equilibrium alone controlled the overall extraction rate. When an overall mass transfer coefficient of 1/10 smaller in magnitude than the estimated one was used for the calculation, the effect of mass transfer began to appear in the overall extraction process.

The lines in Fig. 6 show predicted curves at various flow rates. Since equilibrium is held, predicted extraction curves fall on the same line when plotted against amount of carbon dioxide. The adsorption equilibrium constant K was therefore independent of the flow rate.

The adsorption equilibrium constants obtained by the above procedure are shown on a van't Hoff plot in **Fig. 9**, which gives an approximate heat of adsorption of ΔH = 15 – 25 kJ/mol.

A the comparison between experimental data and predicted curves are shown in **Fig. 10** for various pressures and in **Fig. 11** for various temperatures. As can be seen, the predicted curves agree well with experimental data by using the adsorption equilibrium constant in Fig. 9.

Conclusions

The extraction rate of peppermint oil by supercritical carbon dioxide was measured. The extraction rate of *l*-menthol was much smaller than that expected from solubility. The extraction rate was analyzed by a mathematical model accounting for both the local adsorption equilibrium of essential oil on lipid and mass transfer. Comparison between experimental data and the model gave the adsorption equilibrium constant. The extraction curves were simulated well by the model.

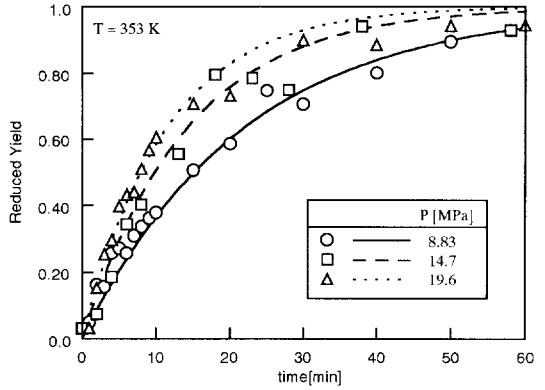

Fig. 10 Comparison between experimental data and predicted curves at various pressures

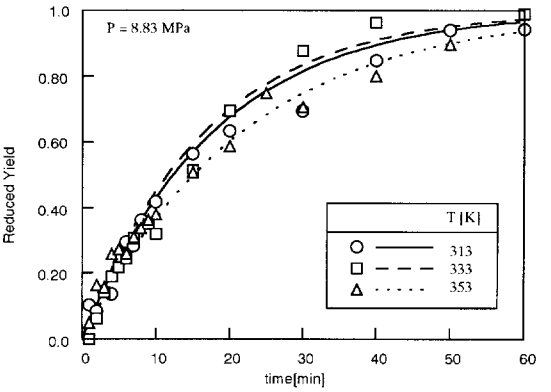

Fig. 11 Comparison between experimental data and predicted curves at various temperatures

Acknowledgment

This work was partly supported by the Japan Society for Promoting Sciences (JSPS) and a Grant-in-Aid for Scientific Research (No. 04238106) from the Ministry of Education, Science and Culture, Japan. The authors are grateful to Professor Oner Hortacsu (Bogazici University, Turkey) and Professor Benjamin J. McCoy (University of California Davis, USA) for helpful discussions, and also to Misses K. Nakamura and J. Muguruma for experimental assistance.

Nomenclature

a_1, a_2	=	eigenvalues defined in Eq. (20)	[-]
a_p	=	specific surface area	[1/m]
A	=	quantity defined by Eq. (21)	[-]
b, c	=	parameters defined in Eq. (22)	[-]
Bi	=	Biot number (= $k_f h / D_e$)	[-]
C	=	solute concentration in CO_2 in bed void volume	[kg/m^3]
C_i	=	solute concentration in pore volume of leaf	[kg/m^3]
$\overline{C}_i$	=	average value of C_i	[kg/m^3]
C_s	=	solute concentration in leaf	[kg/m^3 of solid fraction of leaf]
$\overline{C}_s$	=	average value of C_s	[kg/m^3 of solid fraction of leaf]
C_0	=	total solute concentration	[kg/m^3]
D_{AB}	=	binary diffusion coefficient	[m^2/s]
D_e	=	effective intraparticle diffusion coefficient	[m^2/s]
F	=	cumulative fraction of solute extracted	[-]
h	=	half-thickness of leaf	[m]
ΔH	=	apparent heat of adsorption based upon K	[kJ/mol]
k_a	=	adsorption rate constant	[1/s]
k_f	=	external mass-transfer coefficient	[m/s]
k_p	=	combined mass-transfer coefficient	[m/s]
K	=	equilibrium adsorption constant	[-]
Q	=	mass flow rate of supercritical CO_2	[kg/s]
t	=	time	[s, min]
x	=	dimensionless solute concentration in effluent (C/C_0)	[-]
x_i	=	dimensionless solute concentration in pore (C_i/C_0)	[-]
x_s	=	dimensionless solute concentration in leaf (C_s/C_0)	[-]
y	=	coordinate in slab	[m]
α	=	void fraction in bed	[-]
β	=	porosity of leaf	[-]
ϕ	=	dimensionless mass-transfer coefficient ($k_p \tau$)	[-]
θ	=	dimensionless time (t/τ)	[-]
μ	=	viscosity of fluid	[kg/m·s]
ρ	=	density of fluid	[kg/m^3]
ρ_p	=	apparent density of leaf	[kg/m^3]
ρ_s	=	density of solid part of leaf	[kg/m^3]
τ	=	total bed volume / volumetric flow rate	[s]

Literature Cited

1) Barton, P., R.E. Hughes, Jr., and M.M. Mussein: *Proc. 2nd Int. Symp. on Supercritical Fluid,* p.279-282 (1991)
2) Brogle, H.: *Chem. Ind.,* **19,** 385-390 (1982)
3) Brunner, G.: *Ber. Bunsenges. Phys. Chem.,* **88,** 887-891 (1984)
4) Goto, M., J.M. Smith, and B.J. McCoy: *Ind. Eng. Chem. Res.,* **29,** 282-289 (1990)
5) Goto, M., J.M. Smith, and B.J. McCoy: *Chem. Eng. Sci.,* **45,** 443-448 (1990)
6) Maier, M. and K. Stephan: *Chem. Ing. Tech.,* **56,** 222 (1984)
7) Ozer. E., Platin, S., Akman, U, and O. Hortacsu: AIChE Annual Meeting, Florida 5cf (1992)
8) Peker, H., M.P. Srinivasan, J.M. Smith, and B.J. McCoy: *AIChE J.,* **38**, 761-770 (1992)
9) Reid, R.C., J.M. Prausnitz and B.E. Poling: "The Properties of Gases & Liquids," 4th ed., McGraw-Hill, New York (1987)
10) Srinivasan, M.P., J.M. Smith, and B.J. McCoy: *Chem. Eng. Sci.,* **45,** 1885-1895 (1990)
11) Srinivasan, M.P., J.M. Smith, and B. J. McCoy: *Chem. Eng. Sci.,* **46,** 371-374 (1991)
12) Wakao, N. and S. Kaguei: "Heat and Mass Transfer in Packed Beds", Gordon and Breach (1985)